Assessment of Water Clarity within Dokan Lake Using Remote Sensing Techniques

Hasti Shwan Abdullah
M.Sc. in Water Resources
Engineering
Faculty of Engineering /University of
Sulaimani-Sulaimani-Iraq
hasti.shwan@gmail.com

Mahmoud Saheh Al-Khafaji
Assistant professor
Department of Building and
Construction Engineering
University of Technology
41100@uotechnology.edu.iq

Hekmat M. Ibrahim
Lecturer
Faculty of Engineering /University of
Sulaimani-Sulaimani-Iraq
hekmatmustafa1968@gmail.com

ABSTRACT

It is impractical to monitor lakes water quality by conventional field methods because of expense and time consuming. Satellite image is more convenient to be used to collect the required data for monitoring and assessing lakes water quality. This study aims to develop a water clarity estimation model based on remote sensing and GIS techniques to estimate and assess the water clarity within Dokan Lake in Kurdistan Region of Iraq. Twenty points in the lake were selected and studied at autumn and spring seasons. For assessing water clarity, the Secchi Disk Transparency (SDT) and the Trophic State Index (TSI) were used at these twenty stations in the lake. Multiple linear regression is used to obtain mathematical models for estimating the water clarity depending on spectral reflectance of Landsat 8 OLI. In this study, the new band (coastal blue) of Landsat 8 OLI has been undertaken in developing of the monitoring models. Moreover, new Independent Component Analysis (ICA) and new 7 band ratios with 16 band combinations have been investigated. The obtained highest determination coefficient values for SDT and TSI were 0.98 and 0.87 for autumn season and 0.95 and 0.97 for spring season respectively. Generally, for spring season, the performance of all models is reduced due to seasonal change, variance of parameters and other factors. The developed models were used to map the water clarity distribution within Dokan Lake. The results of the developed SDT and TSI models showed that the correlation of all bands of Landsat 8 OLI is appropriate to monitor the water clarity. These models can be effectively used to monitor the water clarity within the lake with conservation of time efforts and cost.

Keywords: Clarity, Trophic State Index, Secchi Disk Transparency, Image Processing, Landsat 8, GIS.

تقييم نقاوة المياه في بحيرة دوكان باستخدام تقنيات التحسس النائي

حكمت مصطفى ابراهيم
مدرس
جناح الهندسة- جامعة السليمانية – السليمانية -
العراق

محمود صالح مهدي
استاذ مساعد
قسم هندسة البناء والانشاءات
الجامعة التكنولوجية / بغداد- العراق

هاستي شوان عبد الله
ماجستير في هندسة الموارد المائية
جناح الهندسة- جامعة السليمانية – السليمانية -
العراق

الخلاصة

تعد عملية مراقبة اجزاء كبيرة من البحيرات باستخدام الطرق الحقلية التقليدية امراً غير عملياً بسبب الكلفة واستهلاك الوقت. إن استخدام المرئيات الفضائية اكثر كفاءة في جمع البيانات المطلوبة لمراقبة وتقييم نوعية المياه في البحيرات. تهدف هذهِ الدراسة الى حساب وتقييم نقاوة المياه في بحيرة دوكان من خلال تطوير وتطبيق نموذج حساب لنقاوة المياه يعتمد على تقنيات التحسس النائي ونظم المعلومات الجغرافية لبحيرة دوكان في اقليم كردسان في العراق. عشرون نقطة في البحيرة تم اختيارها ودراستها في فصلي الخريف والربيع.. تم استخدام شفافية قرص سايكي (SDT) ومؤشر الاثراء الغذائي (TSI) في

عشرون نقطـة لتقييم نقاوة المياه في بحيرة دوكـان. تم استخدام نموذج الانحسار المتعدد لإيجاد نموذج رياضـي لحسـاب نقـاوة المياه اعتمـاداً على الانعكاسية الطيفية للمرئيات الفضـائية للقمر Landsat 8 OLI. في هذهِ الدراسـة تم استخدام الحزمـة الطيفية الجديدة (الحزمـة الطيفية الزرقاء Coastal Blue) لمرئيات القمر الصناعي Landsat 8 OLI في تطوير نماذج المراقبة. فضـلا عن ذلك تم استخدام تحليل المكونات المستقلة (ICA) بسبع نسب حزمية مع ستة عشر تركيبـة حزمية. أن اعلى قيم معامل تحديد لل SDT وTSI تم الحصـول عليها هي 0.98 و0.87 لفصل الخريف و 0.95 و 0.97 لفصل الربيـع على التوالي. بصـورة عامـة، نقل كفائـة كل النمـاذج الحسـابية عند تطبيقهـا في فصل الربيع بسبب التغيرات الموسمية وتباين العنـاصر وعوامل اخرى. تم استخدام النمـاذج المطورة في رسم خرائط توزيع نقاوة المياه في بحيرة دوكان. بينت نتائج نمـاذج SDT وTSI ان ترابط كل الحزم الطيفية لمرئيات القمر الصناعي Landsat 8 OLI مناسبـة لمراقبـة نقاوة المياه. إن تلك النمـاذج يمكن اسنخدامها بكفاءة لمراقبة نقاوة المياه في البحيرة مع توفير الكثير من الجهد والكلفة.

1. INTRODUCTION

   Water quality monitoring is the systematic collection and evaluation of data about the chemical, physical, and biological quality of the water bodies, and assesses how external changes in both natural and anthropogenic affect the water quality. To get a true picture about the nature of the river and lake water, it is necessarily required to measure the quantity and quality of water through water quality monitoring, which implemented in many methods and techniques. The traditional method of water quality monitoring, is collecting and analyzing water samples and testing them in laboratory which requires more times and costs. Recently, with advance and increase in monitoring technology, new techniques and methods are developed for assessing water quality such as Remote Sensing (RS) and Geographical Information System (GIS) that overcomes through using satellite data to monitor water quality to reduce time and cost for the process, and to increase the accuracy of results. **Ming, *et al*., 1996,** established an integrated water quality monitoring system data which obtained from SPOT (French Satellite for observation of Earth: Satellite Pour l'Observation de la Terre) data with GIS techniques in central Taiwan. Also, **Olmanson, *et al*., 2002,** developed an image processing and classification procedure based on a strong relationship between Landsat TM bands 1 and 3 and Secchi Disk Transparency (SDT).

Remote sensing and GIS have a potential to monitor spatial variation in water quality over large areas. **Doxaran, *et al*., 2005,** obtained linear relationships and a high correlation between the concentrations of colored dissolved organic and suspended (total, organic and inorganic) matter and remote-sensing Reflectance (Rrs) measurements in the Tamar estuary (south-west UK). Remote sensing of lake water is often limited to high spatial resolution satellites such as Landsat, which have limited spectral resolution. The first four bands of Landsat 7-ETM satellite data were correlated by **Alparslan, *et al*., 2007,** with chlorophyll-a, suspended solid matter, SDT and total phosphate to assess water quality at Omerli dam, Istanbul city, Turkey.

Many studies have used the regression technique to correlate the water quality parameters with satellite image data. Most of studies used and tested many kind of water quality parameters such as chlorophyll – a, Secchi Disk Transparency (SDT) and phosphorous by using Landsat TM, ETM or Spot Data. **Mahdi, *et al*., 2009,** used remote sensing techniques to monitor the Trophic State Index (TSI) within Al Huweizah Marsh using satellite images of Landsat-7 TM for 1990 and Landsat-7 ETM for 2000, 2002, and 2006 the results shows that the developed model can be effectively used to estimate the TSI distribution pattern within the marsh.

Knowledge of the spatial distribution of different biological, chemical and physical variables is essential in environmental water studies as well as for resource management, **Meer, *et al*., 2006**.

Dokan Lake is one of the main sources of drinking, irrigation water and power generation in the province of Kurdistan Region, Iraq and especially to the province of Sulaimani, Therefore, this study aims to ascertain the feasibility of estimating water clarity and its spatial distribution using Landsat 8 OLI imagery combined with in situ data from Dokan Lake.

The present study focuses on modelling of SDT and Trophic State Index (TSI) using remote sensing and GIS techniques. The SDT measured to calculate TSI and developing models from Landsat 8 OLI reflectance bands which have not used before in previous studies such as Coastal Blue of Landsat 8. A new ratios and combinations of spectral bands of Landsat 8 OLI and their transforms such as Independent Component Analysis (ICA), Minimum Noise Fraction (MNF), are used in this study.

2. METHODOLOGY

Generally, the methodology of carrying out this study can be divided into two parts, theoretical approach which concerns reviewing the national and international historical background researches that used different techniques to find and evaluate the water clarity for local and international lakes and that related to the use of remote sensing and GIS techniques in this issue and experimental approach which concerns the field work and data analysis. **Fig. 1** shows the flow chart of carrying out the present study.

3. MATERIALS AND METHODS

3.1 Study Area

Dokan Lake is located in Iraq on the Lower Zab River approximately 295 km north of Baghdad and 65 km southeast of Sulaimani City as shown in **Fig. 2**. It is surrounded by mountains of Sara and Quasar to the southeast, Assos to the northeast, Kosrat to the southwest and Barda Rash to the northwest, **Ararat, *et al.*, 2009**. The reservoir impounded by Dokan Dam which has a total design capacity of 6.870 billion cubic meters at normal operating level of 511 m.a.s.l. (6.140 billion cubic meters is live storage and 0.730 billion cubic meters being dead storage). The current storages are less than this due to over 50 years of sedimentation, **Ali *et al.*, 2003** as cited in **Bilbas, 2014**.

3.2 Water Clarity

Water clarity, or transparency, is commonly measured by using the Secchi disk (SD) and it is reduced by the presence of suspended sediment and Marl ($CaCO_3$), bits of organic matter, free-floating algae, and zooplankton. The Trophic State Index (TSI) is an indicator of the biological productivity which can be calculated based on SDT measurements, Chl-*a* concentrations, and total phosphorus (TP) concentrations measured near the lake's surface. The TSI or the Carlson Index is developed to present the trophic classification of lakes. The TSI calculation in this study is based on the Secchi disk depth as given below:

$$TSI = 60 - 14.41\,(\ell n\,SDT) \quad .... \quad (1)$$

Where SDT is the Secchi depth in meters, and ℓn stands for the natural log of a number. Once the TSI have been calculated, it is easy to compare the results to other lakes or recalculate the value each year to see whether there appears to be any upward or downward trend in the lake, **Carlson, 1977**.

Many studies show that TSI and SDT have correlation with satellite image and can be estimated by remote sensing. The estimated SDT can be converted to Carlson's trophic state index based on calculation and correlation of TSI with spectral responses.

3.3 Remote Sensing

The detection of electromagnetic energy can be performed either photographically or electronically. Imagery can be expressed in four dimensions, spectral, temporal, radiometric and spatial resolutions, **Navulur, 2007**. The general processes and elements involved in remote sensing of earth resources are grouped into two basic processes, data acquisition and data analysis processes.

Since 1972, Landsat satellites have continuously acquired space-based images of the Earth's land surface, coastal shallows, and coral reefs. Landsat 8 data are used by government, commercial, industrial, civilian, military, and educational communities throughout the United States and worldwide, **USGS, 2015**. Therefore, the Landsat 8 data have been used in the present study to determine the SDT and TSI of Dokan Lake water.

3.4 Image Pre-processing

The satellite data image processes include two groups, the first is pre-processing and the second is image enhancement and transformations. The pre-processing commonly comprises a series of sequential operations, including geometric correction, atmospheric correction or image registration, normalization, masking (e.g., for clouds, water, irrelevant features), image rectification, and image re-sampling, **Baboo, *et al.*, 2014**. There are two formulas that can be used to convert Digital Numbers (DNs) to radiance; one method uses the Gain and Bias values from the header file. The method converts DNs to at-sensor spectral radiance L, also called top-of-atmosphere radiance:

$$L_\lambda = Gain \times QCal + bias \quad \ldots\ldots\ldots\ldots\ldots\ldots\ldots\ldots\ldots\ldots\ldots\ldots\ldots\ldots\ldots\ldots \quad (2)$$

Where:

L_λ = Spectral Radiance at the sensor's aperture in watts/ ($m^2 \times$ ster$\times$ μm).

$Gain$ = Rescaled gain (the data product "gain" contained in the Level 1 product header or ancillary data record) in watts / ($m^2 \times$ ster$\times$μm).

$QCal$ = the quantized calibrated pixel value in DN.

$bias$ = Rescaled bias (the data product "offset" contained in the Level 1 product header or ancillary data record) in watts/($m^2 \times$ster$\times$μm).

The longer method uses the LMin and LMax spectral radiance scaling factors. Coefficients are provided in one of three band-specific formats: gain and offset; $Grescale$ (also called gain) and $Brescale$ (bias); or radiances associated with minimum and maximum DN values ($Lmax$ and $Lmin$). Any of the three can be used to convert from DN to at-sensor radiance:

$$L_\lambda = \frac{LMAX_\lambda - LMIN_\lambda}{QCALMAX - QCALMIN}(QCAL - QCALMIN) + LMIN \quad \ldots\ldots\ldots\ldots \quad (3)$$

Where:

L_λ = the cell value as radiance.

$QCAL$ = digital number.

$LMIN_\lambda$ = spectral radiance scales to QCALMIN.

$LMAX_\lambda$ = spectral radiance scales to QCALMAX.
$QCALMIN$ = the minimum quantized calibrated pixel value (typically = 1).
$QCALMAX$ = the maximum quantized calibrated pixel value (typically = 255).

New characteristics are added to enhance and automatize ground reflectance retrieval by conversion to top of atmosphere reflectance units, **Goslee (2011)**, as follow:

$$\rho_\lambda = \frac{\pi L_\lambda d^2}{ESUN_\lambda sin\theta} \quad ……………………………………………..……… \quad (4)$$

Where:
L_λ= Radiance in units of W/ (m^2 × sr × μm).
d= Earth-sun distance, in astronomical units.
$ESUN_\lambda$= Solar irradiance in units of W/ (m^2 × μm).
θ= Sun elevation in degrees.
To deduce values for atmospheric parameters from information contained within the image itself rather than using externally-measured data, absolute atmosphere correction is carried out as follow:

$$\rho = \frac{\pi d^2(L - L_{haze})}{T_v(E_{sun} cos\theta_z T_z + E_{down})} \quad …………………………………………… \quad (5)$$

3.5 Image Processing

The objectives of the second group of image processing functions are grouped under the term of image enhancement and transformations. Some of image transformations that can be made by the ENVI software and used in this study are: Minimum Noise Fraction (MNF), Principal Component Analysis (PCA), Independent Component Analysis (ICA), band ratios and indices. **Table 1** shows some spectral indices that used in the present study.
Another process includes the image classification and analysis which are used to digitally identify and classify pixels in the data. Classification is usually performed on multi-channel data sets (A) and this process assigns each pixel in an image to a particular class or theme (B) based on statistical characteristics of the pixel brightness values, CCRS (2014).
The remote sensed data image which used in this study include two Landsat-8 OLI images (path: 169 and row: 35) acquired on 24 October 2014 as an (ID: LC81690352014297LGN00) and 02 April 2015 as an (ID: LC81690352015092LGN00). The images were downloaded from the USGS, Earth Explorer (EE) website. Both images were contained small pockets of clouds, which covered about 0.23% and 7.29% of the autumn and spring seasons image respectively. These values are less than the minimum removing percentage (9%) of full scene of satellite image USGS, 2015, so there is no need of haze of cloud removal. ENVI software has been used for geospatial analysis and spectral image processing of Landsat 8 OLI data imagery.
The images have been geometrically corrected and prepared for atmospheric correction which is carried out to minimize the atmospheric effects through correcting DN values to radiance. To derive a radiance image from uncalibrated image, a gain and offset applied to the pixel values. These gain and offset values are typically retrieved from the image's metadata or received from the data provider. ENVI software provides a tool called radiometric calibration undertakes this process for many data products that are distributed with calibration gain and offset values in the

metadata. Finally, radiance is converted to Surface Reflectance (SR) which represents the reflectance of the surface of the Earth as shown in **Fig. 3**.

Therefore, clouds and other atmospheric components do not affect the surface reflectance spectra. The SR reflectance is unlike the Top-of-Atmosphere (TOA) reflectance which is the reflectance measured by a space-based sensor flying higher than the earth's atmosphere. These TOA reflectance values include contributions from clouds and atmospheric aerosols and gases.

Following atmospheric corrections, seven bands of Landsat 8 OLI for each image were extracted as a layer stacking of multispectral bands image. Each corrected image was subset to much small study area to be easy for the selection of ground control points (GCP) that used in correction and study area subset images. As images undergo unsupervised classification process, pixels were grouped based on the reflectance properties which are known as "clusters". Each cluster with different land cover classes were identified and multiple clusters which represent a single land cover class merged into a land cover type in order to subset and mask out the wetted bodies from satellite data as illustrated in **Fig. 4**.

To ensure the accuracy of the classification, an accuracy assessment of the land use / land cover map was carried out to compare certain pixels in classified subsets with reference pixels through using supervised classification which determined by integrated approach based on technique which is used to improve the accuracy of predictive models by ENVI software.

Finally, transformation process to the satellite image (extracted studied area) was provided, which typically involve the manipulation of multiple bands of data. Before transformation, image enhancement methods are applied separately to each band of a multi-spectral image such as contrast enhancement, linear contrast stretch, and spatial filtering.

Image transformation in this study creates an output dataset where each output band is a linear combination of all the input bands. The first transform is Independent Component Analysis method (ICA) which works well with hyperspectral data because it is more likely to treat sparse targets as important features. However, ICA method can take a significantly longer time to process. The next method is PCA which creates a number of PC bands, which are linear combinations of the original spectral bands that are uncorrelated. It can be calculated the same number of output PC bands as input spectral bands. The first PC band contains the largest percentage of data variance and the second PC band contains the second largest data variance, and so on. Final transformation method is MNF which is a linear transformation uses separate PCA rotations to segregate noise in the data and to reduce the dimensionality of the original dataset.

3.5.1 Band Ratios

Band Ratios which enhance the spectral differences between bands were used in the present study to increase and provide more independent variables for the models and to reduce the effects of topography. Dividing one spectral band by another produces an image that provides relative band intensities and enhances the spectral differences between bands. One of the band that have been used is Coastal Blues which is Landsat 8 OLI's new band that not available in Landsat 7. It was used with other spectral bands whether as a combination or band ratios such as (C/B), (C/G), (C/R), (C/NIR), (B/C), (B/G), (B/R), (B/NIR), (G/C), (G/B), (G/R), (G/NIR), (R/C), (R/G), (R,B), (R/NIR), (NIR/C), (NIR/B), (NIR/G), (NIR/R), (B+C), (B+G), (B+R), (B+NIR), (G+C), (G+R), (G+NIR), (R+C), (R+NIR), (C+NIR), (B+G+C), (B+G+R), (B+G+NIR), (B+R+NIR), (B+R+C), (B+C+NIR), (G+C+R), (G+C+NIR), (R+C+NIR), (G+R+NIR), (B+G+R+NIR), (C+B+G+R), (C+B+G+NIR), (C+G+R+NIR), (C+B+R+NIR), (C+B+G+R+NIR), (B/NIR+C), (B/NIR+B), (B/NIR+G), (B/NIR+R), (B/NIR+NIR), (B/R+C), (B/R+B), (B/R+G), (B/R+R), (B/R+NIR), (NIR/B+C), (NIR/B+B), (NIR/B+G), (NIR/B+R) and

(NIR/B+NIR). Then the spectral indices are combinations of surface reflectance at two or more wavelengths that indicate relative abundance of features of interest. Vegetation index (NDVI) is the most popular type, but other indices such as (LSWI), (MNDWI), (MSI), (NBR), (DVI), (IPVI), (NDMI) and (RVI) are available for water features which are used in this study.

3.6 Statistical Analysis

The statistical process focuses at the nature of statistical relationship between water quality and spatial response of satellite image for predicting the parameters. This process includes two parts, the first part is correlations, which examines linear relationships founds in the data that used to construct a scatterplot in a symmetric manner. While the second part, regression, considers the relationship of a response variable as determined by one or more explanatory variables.

A statistic that quantifies the strength of the linear relationship between the two variables is the correlation coefficient. The Pearson product-moment correlation coefficient is more widely used in measuring the association between two variables, **Berthouex, *et al.*, 2002**, and it has been taken into account in this study as well.

There are three types of regression, simple, multiple and nonlinear regressions that can be used to determine the relationship between two or more variables, **Yan, *et al*., 2009**. The simple and multiple regressions were used in this study.

Many criteria for choosing subset size have been proposed and based on the principle of parsimony which suggests selecting a model with small residual sum of squares with as few parameters as possible, **Rawlings, *et al*., 1998**. The commonly used criteria are coefficient of determination (R^2), adjusted R^2 (R^2_{adj}), residual mean square MS_{res}, Mallows C_p Statistic, Akaike Information Criterion (AIC), Schwarz Bayesian Criterion (SBC), …, etc, **Weisberg, 2005**. In order to evaluate the performances of the developed models and to provide an indication of goodness of fit between the observed and calculated values, coefficient of determination (R^2), were used for each model investigated in this study.

The atmospherically corrected water masked Landsat 8 OLI images were used for water quality spatial analysis in this study. Twenty measurements points were located on the image based on the UTM coordinates determined with a GPS during water sampling and extracted the spectral band of used image that mentioned before as independent variables, in ArcGIS Desktop software, to be used in correlation and regression modeling. Only the single pixel value for each sampling station was extracted.

A Pearson correlation matrix was first developed to determine the strengths of correlation between water clarity parameters and spectral bands. Multiple linear regression methods were subsequently used to further explore the correlation between water clarity parameters and spectral bands. The spectral band values at each measurement station were extracted from images for use as independent variables in bivariate regression models. Only the first seven bands that known as OLI were used for the analysis based on examination of the data. Independent variables include 14 surface reflectance bands, 7 PCA bands, 7 ICA bands,7 MNF bands, 20 band ratios, 26 band combinations and finally 9 indices. Dependent variables that were analyzed include clarity of water by indication of SDT, and TSI. All statistical analysis in this study has been done using SPSS computer software.

Regression models were chosen to estimate both SDT and TSI in Dokan Lake based on correlation coefficients and coefficients of determinations. Maps have been produced for measured versus computed water clarity values and visual interpretation of parameters.

4. EXPERIMENTAL WORK

Theoretical study of any phenomena, often, requires verification of its results empirically based on experimental measurement, field and laboratory results. The experimental works in this study include measurement of SDT in the Dokan Lake. First, twenty sampling stations were established on the map of the lake. Sampling stations were selected in the study area at slightly equal distance from each other. The number of stations was selected according to the criteria of specifying the sample in order to sufficiently estimate the clarity of a water body of this size. Second, a GPS receiver (Garmin 62S) was used in a boat to locate each sample station in the lake for collecting the water samples.

Twenty samples were taken from predetermined stations at two different dates. These twenty stations consisted ground reference data of SDT measurement in a day which was coincident with the acquisition date of Landsat 8 image which overpass and capture image. The short difference between the measurement and image capturing time does not affect the accuracy of the analyses results because the change of water clarity in several hours is very rare.

The SDT measurements were carried out on 24 October of 2014 as an autumn season and on 02 April 2015 as a spring season. For autumn season, the sampling day was sunny with a temperature range of 13 to 22 C^0 and a slight wind with a speed of 2.1 m/s coming from 159^0 N. On the measurement day, inflow discharge was 70 m^3/s same as the rate of outflow discharge which was less than the average daily because there was no precipitation in the catchment area. While for spring season, the sampling day was partly overcast but there is no cloud at the same area of the lake with a temperature in the range 9 to 19 C^0 and a slight wind coming with the speed of 1.6 m/s from the 146 N^0. The inflow discharge to the lake was 285 m^3/s which is higher than the rate of outflow discharge and less than the average daily because there is no precipitation in the catchment area. The stations of sampling on October 24th, 2014 and April 2nd, 2015 in Dokan Lake are shown in **Fig. 5**. SDT measurements and TSI that computed from SDT for twenty station points of Dokan Lake water for autumn and spring seasons are shown in **Table 2**.

5. RESULTS AND DISCUSSION

Satellite image data undergoes several processing and transformation to develop water clarity estimation model by using statistical analysis. In this study, the processes depend on the spectral reflectance characteristics of the water in OLI bands of the Landsat 8 spectral bands and comparison of the water clarity values that obtained from the developed models with the measured field data.

The surface reflectance of Landsat 8 OLI bands for selected stations in Dokan Lake at October 24th, 2014 and April 2nd, 2015 are shown in **Fig. 6**.

The SDT and TSI are tested and modeled in Dokan Lake for two different seasons of the year (autumn and spring) as shown in **Table 3**. After processing the images, the multiple linear regressions were used to establish the relationship between the water clarity parameters as dependent variables and Landsat 8 OLI images spectral data as independent variables. Spectral data of autumn and spring images and in situ measurement data on October 24th, 2014 and April 2nd, 2015 of water clarity parameters correlated and multiple linear regression models were developed and the models of the highest R^2 were selected for estimating the water clarity parameters, SDT and TSI, as shown in **Table 3**.

For autumn season, the SDT model shows that it is strongly correlated with the NDMI of Landsat 8 OLI data with R^2 of 0.96. Furthermore, result of the TSI model shows that it is highly correlated with R/NIR and LSWI which gives R^2 value of 0.94. On the other hand, for spring season, the results show that the SDT is strongly correlated with the MNDWI, C/G and G/R of

Landsat 8 OLI data, and having highest R^2 value of 0.95. In addition, the result of TSI model shows a high correlation with R/C and MNDWI which give R^2 value of 0.97. In autumn season, SDT values within the lake are increased from inlet toward Dokan Dam. In spring season, generally, the values of SDT and TSI are remained as in autumn season without a significant change.

The SDT and TSI were computed and the spatial distribution of their values were mapped through applying the developed models on the Landsat 8 OLI image of Dokan Lake for autumn and spring seasons as shown in **Fig 7**.

To check the generality of the developed models, the models that developed for autumn season data have been tested by using the spring season data and vice versa.

The best models that have been developed for autumn season data on October 24th, 2014 were used to predict the water clarity parameters of Dokan lake water for spring season data on April 2nd, 2015. New coefficients of determination (R^2) have been calculated for each model as shown in **Table 4**. The results show that the values of R^2 are decreased to 0.75.

On the other hand, the best models that have been developed for spring season data on April 2nd, 2015 were used to predict the water clarity parameters of Dokan lake water for autumn season on October 24th, 2014. A new coefficient of determination (R^2) has been calculated for each model as shown in **Table 4**. The results show that the values of R^2 are decreased to 0.44 and 0.68 for SDT and TSI respectively. The main factor which causes to change the performance of models is high variation of all data when the season is changed. As clear from the results, TSI model can be used as general model for all seasons of the year.

6. CONCLUSIONS

Results analyses of experimental works, remote sensing processing works, and SDT and TSI models in the present study show that some bands of Landsat 8 OLI can be correlated with water clarity parameters. Statistical analysis show that the water clarity within Dokan Lake can be effectively correlated with the Coastal Blue band with its combinations and band-ratios, independent component analysis (ICA) and minimum noise fraction (MNF).

Statistical analysis of the SDT models of autumn season shows that SDT is strongly correlated with the NDMI of Landsat 8 OLI data. Furthermore, analysis of the TSI models shows that it is highly correlated with R/NIR and LSWI. While, for the spring season, the results show that SDT is strongly correlated with the MNDWI, C/G and G/R of Landsat 8 OLI data. In addition, the result of TSI model shows a high correlation with R/C and MNDWI. In autumn season, SDT values within the lake are increased from inlet toward Dokan Dam. In spring season, generally, the values of SDT and TSI are remained as in autumn season without a significant change.

The results show that Secchi Disk Transparency (SDT) and Trophic State Index (TSI) parameters have a high correlation with reflectance bands of Landsat 8 OLI and can be modeled precisely. The obtained results of TSI parameter prove that it can be modeled and to be used for a whole year.

REFERENCES

- Ali, S. S. & Salley, S. K. R., 2003. Numerical Groundwater Flow Modeling for The Intwrgranular Aquifer in Sarsian Sub-Basin, Dokan Lake, Iraqi Kurdistan Region. Journal of Zankoy Sulaimani-Part A, 15(1), pp. 125-141.
- Alparslan, E., Aydöner, C., Tufekci, V. & Tüfekci, H., 2007. Water quality assessment at Ömerli Dam using remote sensing techniques. Environ Monit Assess, Volume 135, pp. 391-398.

- Ararat, K., Hassan , N. A. & Abdul Rahman, S., 2009. Key Biodiversity Survey of Kurdistan, Northern Iraq, Sulaimani, Kurdistan, Iraq: Nature Iraq Report.

- Baboo, C. D. S. S. & Thirunavukkarasu, S., 2014. Geometric Correction in High Resolution Satellite Imagery using Mathematical Methods: A Case Study in Kiliyar Sub Basin. Global Journal of Computer Science and Technology: Graphics & Vision, 25(1).

- Berthouex, P. M. & Brown, L. C., 2002. Statistics for Enviromental Engineers. 2 ed. Boca Raton, London, New York, Washington, D.C.: Lewis Publishers.

- Bilbas, A. H. A., 2014. Ecosystem Health Assessment of Dukan Lake, Sulaimani, Kurdistan Region of Iraq. Erbil: Salahaddin University.

- Carlson, R. E., 1977. A trophic state index for lakes. Limnology and Oceonography , pp. 361-369.

- CCRS, C. C. f. R. S., 2014. Tutorial: Fundamentals of Remote Sensing. Available at: http://www.nrcan.gc.ca/earth-sciences/geomatics/satellite-imagery-air-photos/satellite-imagery-products/educational-resources/9309
[Accessed 3/ 7/ 2015].

- Doxaran, D., Cherkuru, R. C. N. & Lavender, S. J., 2005. Use of reflectance band ratios to estimate suspended and dissolved matter concentrations in estuarine waters. International Journal of Remote Sensing, 26(8), pp. 1763-1769.

- Goslee, S. C., 2011. Analyzing Remote Sensing Data in R: The landsat Package. Journal of Statistical Software, 43(4), pp. 1-25.

- Mahdi, M. S., Ziboon, A. R. T. & Al Zubaidy,R. Z., 2009. Remote Sensing Model for Monitoring Trophic State of Al Huweizah Marsh. Engineering and Technology Journal Vol. 28, No. 16, 2010.

- Meer, F. D. v. d. & Jong, S. M. d., 2006. Image Spectrometry ; Basic Principle and Prospective applications. Third Edition ed. Donrecht, The Netherlands: Springer.

- Ming, S. Y., Carolyn , J. M. & Robert, M. S., 1996. Adaptive Short-Termm Water Quality forecasts Using Remote Sensing and GIS. AWRA Symposum on GIS and Water Resources, Issue Sept 22-26.

- Navulur, K., 2007. Multispectral image analysis using the object-oriented paradigm. First Edition ed. Boca Raton, FL: CRCpress, Taylor & Francis Group. LLC.

- Olmanson, L. G., Bauer, M. E. & Brezonik, P. L., 2002. Use of Landsat Imagery to develop a water quality ATLAS of Minnesota's 10,000 lakes. USA, Pecora 15/Land Satellite Information IV/ISPRS Commission I/FIEOS.

- Rawlings, J. O., Pantula, S. G. & Dickey, D. A., 1998. Applied Regression Analysis: A Research Tool,. Second Edition ed. Newyork: Springer.

- UN-ESCWA and BGR (United Nations Economic and Social Commission for Western Asia; Bundesanstalt für Geowissenschaften und Rohstoffe). 2013. Inventory of Shared Water Resources in Western Asia. Beirut.

- USGS, 2015. Landsat—A Global Land-Imaging Mission. Available at: http://remotesensing.usgs.gov. [Accessed 9/6/2015].

- Weisberg, S., 2005. Applied Linear Regression. Third Edition ed. Hoboken, New Jersey.: John Wiley & Sons, Inc.

- Yan, X. & Su, X. G., 2009. Linear Regression Analysis : Theory and Computing. First Edition ed. Singapore: World Scientific Publishing Co. Pte. Ltd.
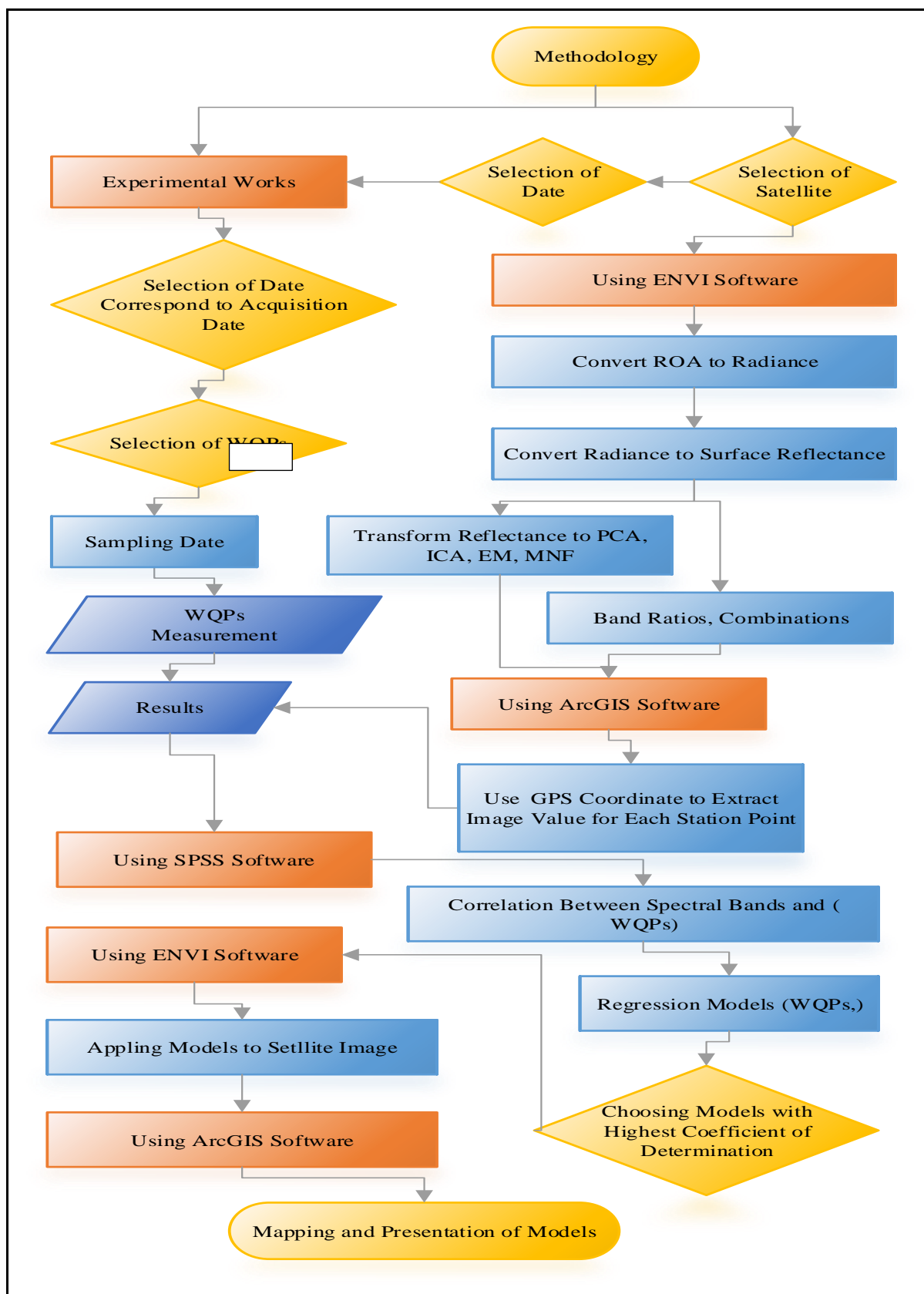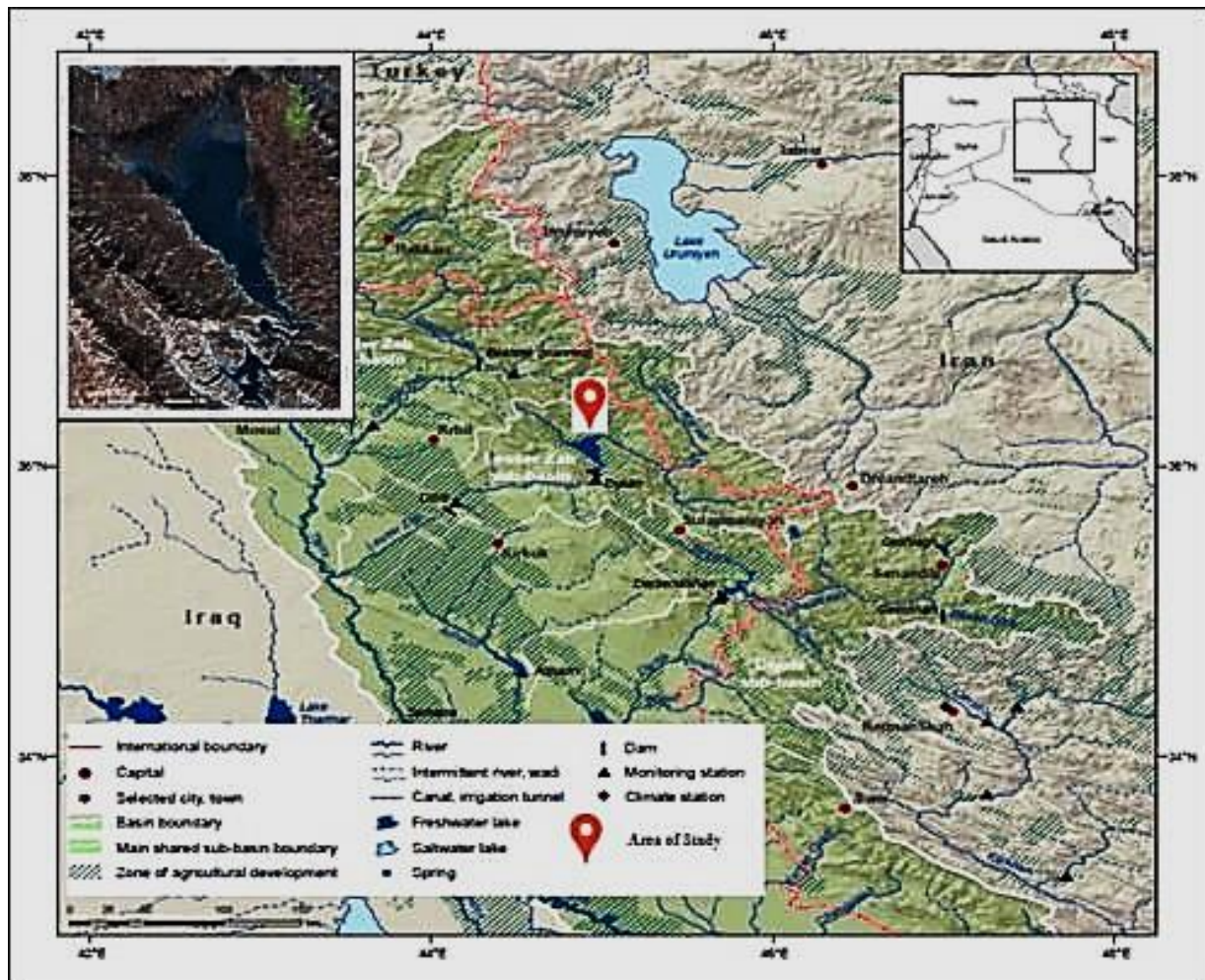
Figure 1. Schematic diagram of the methodology.

Figure 2. Map of Northern Iraq showing the study area cited in, **UN-ESCWA, *et al.,* 2013**.
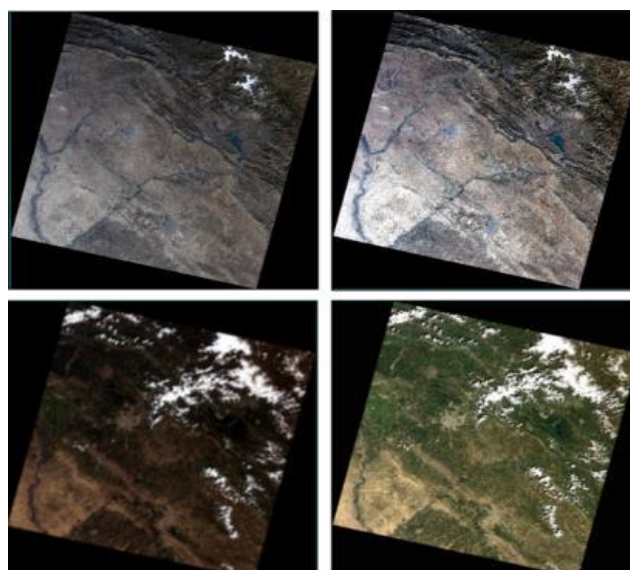

Figure 3. Landsat 8 OLI images of October 24th, 2014 (upper) and April 2nd, 2015 (lower), atmospheric and radiometric correction, (left) before, (right) after pre-processing.
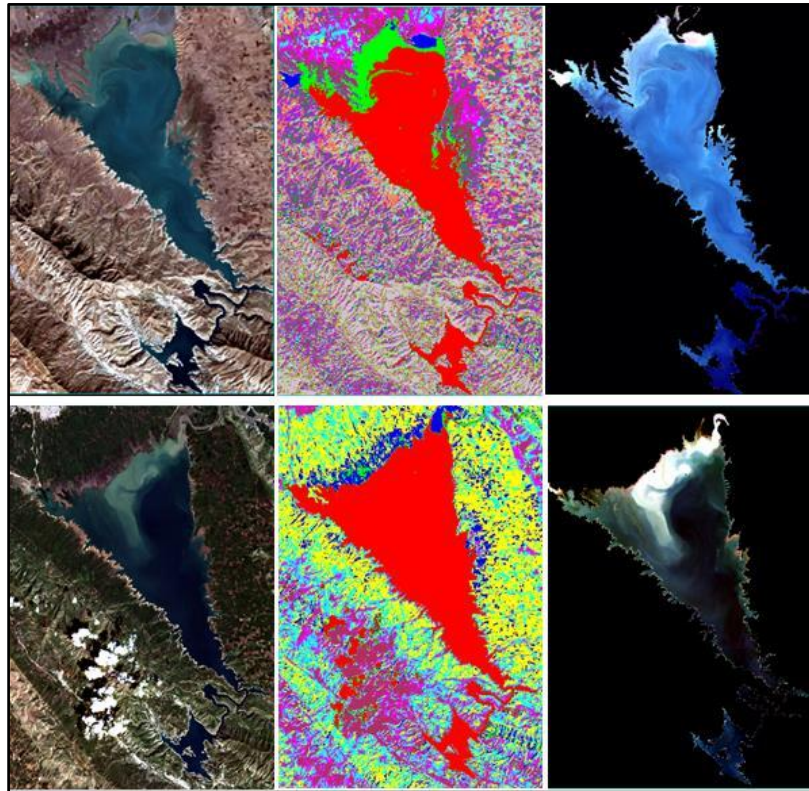
Figure 4. Landsat 8 OLI image for autumn (October 24th, 2014) (upper) and spring (April 2nd, 2015) (lower), after subset (left), unsupervised classification (middle), after extraction of wetted area (right).
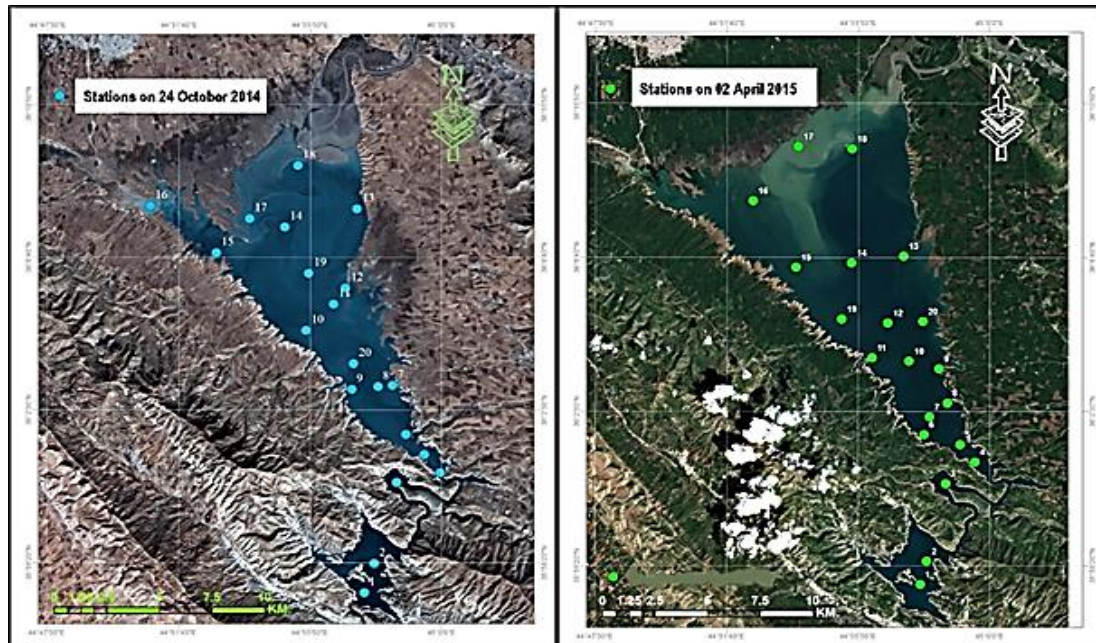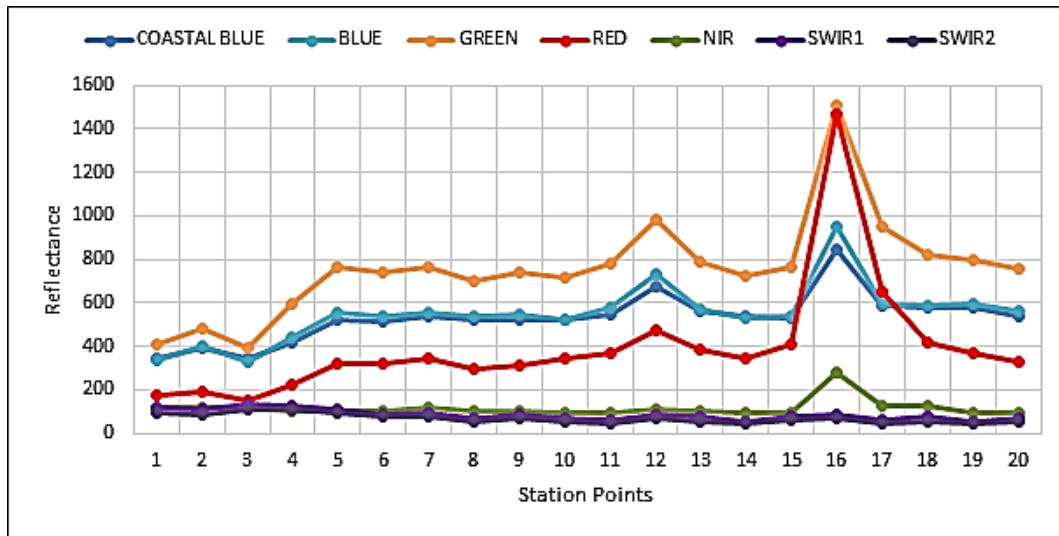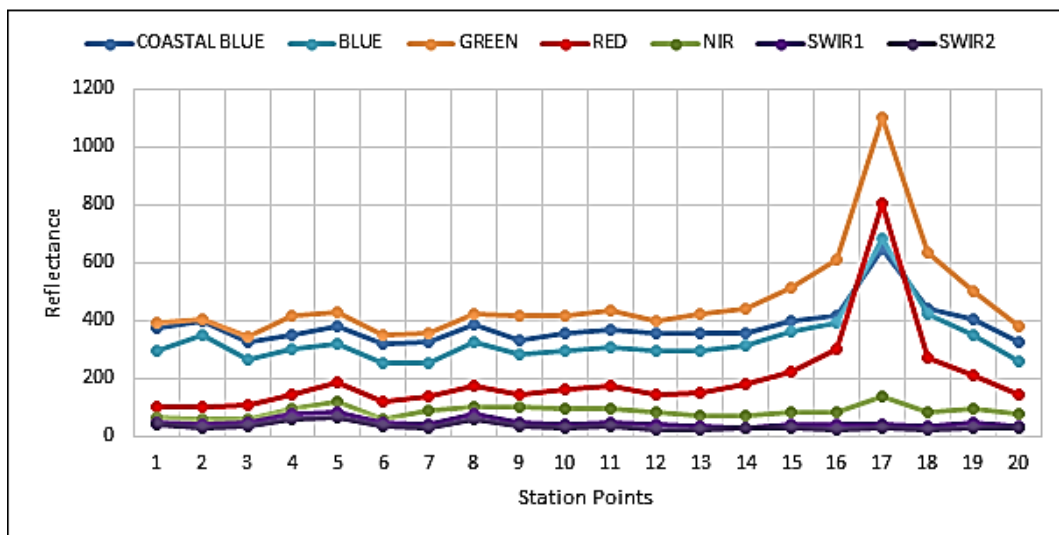

Figure 5. Station points of sampling at autumn (October 24th, 2014) and spring (April 2nd, 2015) within Dokan Lake.

25

a- Autumn (October 24th, 2014).

b- Spring (April 2nd, 2015).

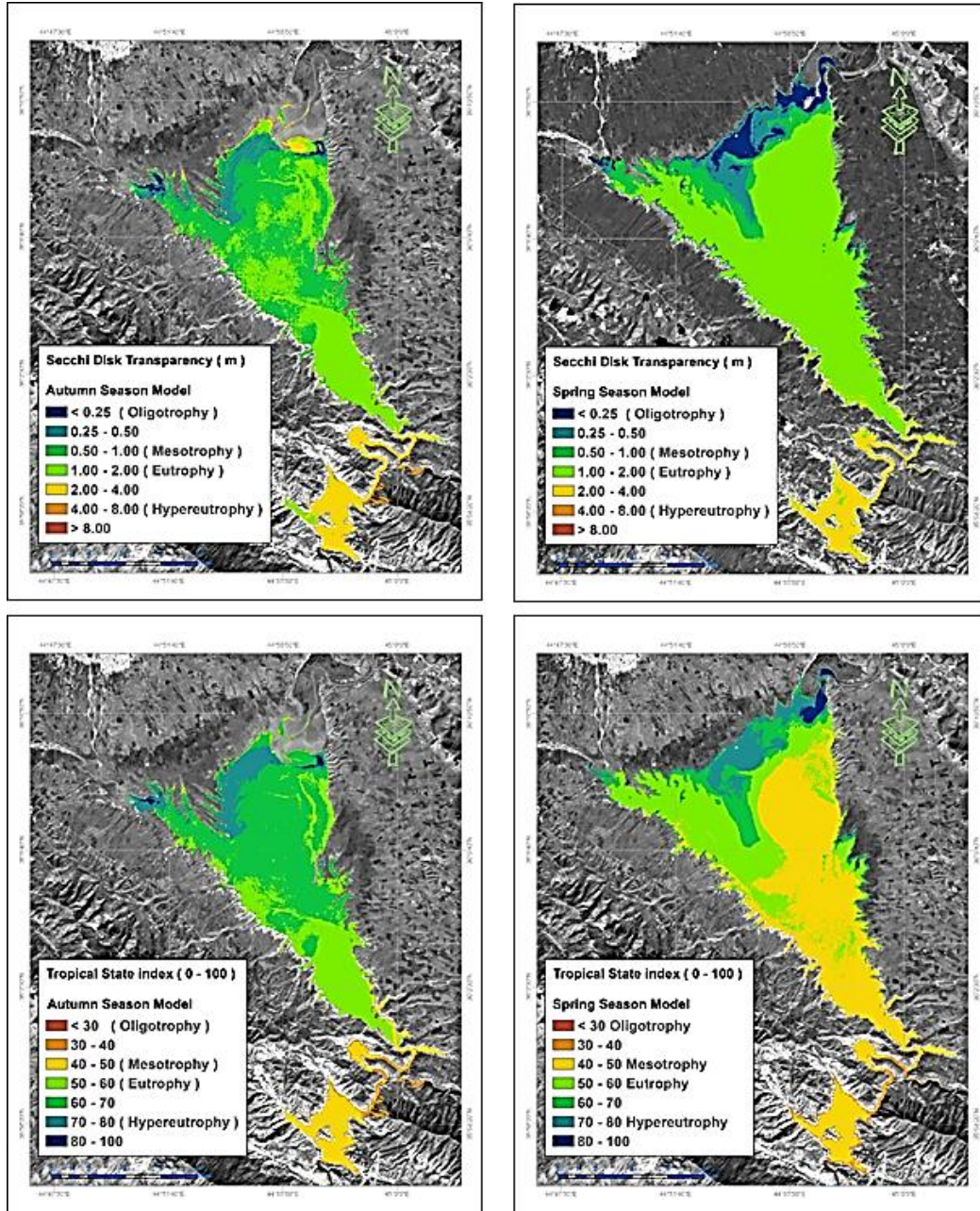**Figure 6**. Surface reflectance of Landsat 8 OLI bands for the selected stations in Dokan Lake at autumn and spring.

26

Figure 7. Distribution of SDT and TSI within Dokan Lake for autumn and spring seasons.

Table 1. Some spectral indices that used in the present study.

No.	Spectral Index	Equation
1	Normalized Difference Moisture Index (NDMI)	$NDMI = (R - NIR)/(R + NIR)$
2	Modification of Normalised Difference Water Index (MNDWI)	$MNDWI = (G - SWIR1)/(G - SWIR2)$
3	Land Surface Water Index (LSWI)	$LSWI = (NIR - SWIR1)/(NIR - SWIR1)$

27

Table 2. Measured SDT and computed TSI for twenty stations within Dokan Lake at autumn (October 24th, 2014) and spring (April 2nd, 2015).

ID	SDT (m)	TSI	Attributes	ID	SDT (m)	TSI	Attributes
October 24th, 2014				April 2nd, 2015			
1	3.3	1	Mesotrophic	1	3.4	42.37	Mesotrophic
2	2.5	2		2	3.25	43.02	
3	3.3	3		3	3.1	43.70	
4	2	4	Eutrophic	4	2.85	44.91	
5	1.55	5		5	2.8	45.16	
6	1.4	6		6	2.65	45.96	
7	1.2	7		7	2.6	46.23	
8	1.5	8		8	2.5	46.80	
9	1.25	9		9	2.45	47.09	
10	1.1	10		10	2.2	48.64	
11	1.1	11		11	1.9	50.75	Eutrophic
12	0.9	12	Blue-green algae	12	2.4	47.38	Mesotrophic
13	1.15	13	Eutrophic	13	2.4	47.38	
14	1.3	14		14	2.1	49.31	
15	0.9	15	Blue-green algae	15	1.45	54.65	Eutrophic
16	0.3	16	Hypereutrophic	16	1.3	56.22	
17	0.4	17		17	0.37	74.33	Hypereutrophic
18	0.9	18	Blue-green algae	18	1.4	55.15	Eutrophic
19	0.4	19	Hypereutrophic	19	1.6	53.23	Hypereutrophic
20	1.55	20	Eutrophic	20	2.1	49.31	Mesotrophic

Table 3. Water clarity models of Dokan Lake for autumn and spring seasons.

Season	Water Clarity Model	R^2
Autumn	$SDT = 3.973 - 5.134\,(NDMI)$	0.96
	$TSI = 35.993 + 5.692\left(\dfrac{R}{NIR}\right) + 18.724\,(LSWI)$	0.94
Spring	$SDT = 1.677 + 2.083\,(C/G) + 0.675\,(G/R) - 3.684\,(MNDWI)$	0.95
	$TSI = 18.826 + 29.115\,(R/C) + 20.364\,(MNDWI)$	0.97

Table 4. Generality of autumn and spring seasons models of SDT and TSI for Dokan Lake (autumn models used for spring data and vice versa).

Season	Water Clarity Model	R^2
Autumn	$SDT = 3.973 - 5.134\,(NDMI)$	0.75
	$TSI = 35.993 + 5.692\left(\dfrac{R}{NIR}\right) + 18.724\,(LSWI)$	0.75
Spring	$SDT = 1.677 + 2.083\,(C/G) + 0.675\,(G/R) - 3.684\,(MNDWI)$	0.44
	$TSI = 18.826 + 29.115\,(R/C) + 20.364\,(MNDWI)$	0.68